European Journal of Radiology 116 (2019) 135–143

Contents lists available at ScienceDirect

European Journal of Radiology

journal homepage: www.elsevier.com/locate/ejrad

Research article

Low-keV virtual monoenergetic imaging reconstructions of excretory phase spectral dual-energy CT in patients with urothelial carcinoma: A feasibility study

David Zopfs[a], Kai Roman Laukamp[a,c], Daniel Pinto dos Santos[a], Marcel Sokolowski[a], Nils Große Hokamp[a], David Maintz[a], Jan Borggrefe[a], Thorsten Persigehl[a], Simon Lennartz[a,b,*]

[a] University Cologne, Faculty of Medicine and University Hospital Cologne, Department of Diagnostic and Interventional Radiology, Kerpener Straße 62, 50937, Cologne, Germany
[b] Else Kröner Forschungskolleg Clonal Evolution in Cancer, University Hospital Cologne, Weyertal 115b, 50931, Cologne, Germany
[c] Department of Radiology, Case Western Reserve University and University Hospitals, 11100 Euclid Ave, Cleveland, Ohio, USA

ARTICLE INFO

Keywords:
Dual energy CT
Spectral CT
Virtual monoenergetic images
Urothelial carcinoma
Contrast media
Excretory phase

ABSTRACT

Objectives: To compare objective and subjective image quality between low keV virtual monoenergetic images (VMI) of the excretory phase and conventional venous phase images derived from spectral dual-energy CT (DECT) in the assessment of urothelial carcinoma.

Methods: 26 consecutive patients with histologically confirmed urothelial carcinoma who received clinically indicated venous- and excretory phase abdominal CT scans were included retrospectively. Attenuation, image noise as well as signal- and contrast-to-noise-ratio (SNR, CNR) in venous and excretory phase CT and excretory phase VMI from 40 to 70 keV were obtained from ROI-based measurements in the following regions: urothelial carcinoma, liver, pancreas, renal cortex, subcutaneous fat, renal vein/artery, portal vein, urinary bladder wall, lymph nodes, prostate/uterus. Subjective vessel contrast and delineation of primary tumor manifestations and distant metastases were rated on 5-point Likert scales.

Results: In comparison to venous phase CT, attenuation and SNR in excretory phase VMI40keV were higher ($p < 0.001$), except for liver parenchyma, where they were comparable ($p = 0.07$ and $p = 0.17$, respectively). Regarding image noise, no significant difference was found between venous phase CT and excretory phase VMI40keV (p-range: 0.08–1.00), except for liver, portal vein and renal artery, where it was lower in VMI40keV ($p < 0.05$). CNR of urothelial carcinoma to circumjacent bladder wall was significantly higher in excretory phase VMI40keV compared to venous phase CT. Subjective vessel contrast and delineation of primary tumor and distant metastases received equivalent or higher Likert scores in excretory phase VMI40keV than in venous phase CT.

Conclusion: This feasibility study indicates that in the assessment of urothelial carcinoma, virtual monoenergetic excretory phase images at 40 keV acquired with spectral DECT could be feasible to maintain subjective and objective image quality as provided by conventional venous phase images. Still, equivalence with regards to metastatic lesion detection requires further investigation before employing this technique in a potential signal-scan, single-bolus approach.

1. Introduction

Urothelial carcinoma accounts for the vast majority of bladder cancers and represents the ninth most frequent type of cancer worldwide [1]. While cystoscopy and urine cytology represent the gold standard for the initial diagnosis of patients with bladder cancer, computed tomography (CT) is the method of choice to rule out primary and secondary lesions of the upper urinary tract and the renal pelvis, as urothelial carcinoma often arises multifocally [2]. Hence, abdominal staging CT protocol for patients with urothelial carcinoma usually

Abbreviations: DECT, dual energy CT; VMI, virtual monoenergetic images; keV, kiloelectron volt; SNR, signal-to-noise ratio; CNR, contrast-to-noise ratio

* Corresponding author.
E-mail address: Simon.Lennartz@uk-koeln.de (S. Lennartz).
@SL_Radiology (S. Lennartz)

https://doi.org/10.1016/j.ejrad.2019.05.003
Received 12 February 2019; Received in revised form 2 May 2019; Accepted 5 May 2019

Table 1
Attenuation and SNR of lymph node, primary urothelial carcinoma, urinary bladder wall, prostate/uterus, poral and renal vein, renal artery, liver and pancreas parenchyma as well as kidney cortex. CNR of primary tumor vs. urinary bladder wall/renal cortex and lymph node vs. retroperitoneal fat. Asterisks indicate statistical significance compared to venous phase CT.

	Venous-phase CT	Excretory-phase VMI_{40keV}	Excretory-phase VMI_{50keV}	Excretory-phase VMI_{60keV}	Excretory-phase VMI_{70keV}	Excretory-phase CT
Attenuation						
Lymph node	75.6 ± 23.9	146.6 ± 43.9 *	103.7 ± 28.6 *	78.5 ± 20.2	63.5 ± 15.7	70.3 ± 14.5
Primary tumor	84.6 ± 26.3	180.6 ± 51.4 *	127.9 ± 32.3 *	96.9 ± 21.3	78.5 ± 15.0	78.7 ± 14.2
Urinary bladder wall	45.8 ± 11.9	105.5 ± 42.0 *	75.1 ± 28.4 *	57.2 ± 21.3 *	46.5 ± 17.7	59.6 ± 12.8 *
Prostate/Uterus	62.2 ± 12.7	151.4 ± 38.5 *	111.5 ± 24.4 *	88.1 ± 16.3 *	74.1 ± 11.6 *	69.3 ± 9.6
Portal vein	152.4 ± 29.0	232.5 ± 49.3 *	161.2 ± 30.9	119.3 ± 20.2 *	94.3 ± 14.1 *	94.0 ± 14.1 *
Renal vein	135.4 ± 30.4 145.1 ± 29.9	208.0 ± 41.0 *	144.7 ± 25.2	107.4 ± 16.1 *	85.3 ± 11.0 *	84.0 ± 10.8 *
Renal Artery	105.5 ± 22.2 85.3 ± 19.2162.	233.8 ± 47.8 *	162.1 ± 29.7	119.9 ± 19.3 *	94.9 ± 13.2 *	93.4 ± 13.5 *
Liver parenchyma	1 ± 29.8	127.0 ± 37.3	100.5 ± 23.9	84.9 ± 16.2 *	75.7 ± 12.1 *	75.4 ± 12.8 *
Pancreas parenchyma	85.3 ± 19.2	132.9 ± 32.2 *	96.5 ± 20.8	75.1 ± 14.8	62.4 ± 12.0 *	62.3 ± 11.5 *
Kidney (cortex)	162.1 ± 29.8	307.3 ± 64.0 *	208.0 ± 40.2 *	149.6 ± 26.3	114.8 ± 18.0 *	112.3 ± 18.1 *
SNR						
Lymph node	6.1 ± 2.0	12.5 ± 6.2 *	9.7 ± 4.5 *	7.8 ± 3.5	6.5 ± 2.8	5.4 ± 2.1
Primary tumor	6.7 ± 1.9	14.1 ± 5.5 *	11.1 ± 3.8 *	9.0 ± 2.9 *	7.6 ± 2.3	5.8 ± 1.6
Urinary bladder wall	3.7 ± 1.1	8.6 ± 4.6 *	6.7 ± 3.3 *	5.4 ± 2.6 *	4.6 ± 2.2 *	4.4 ± 1.5
Prostate/uterus	5.2 ± 1.6	12.9 ± 5.7 *	10.5 ± 4.3 *	8.8 ± 3.3 *	7.6 ± 2.7 *	5.4 ± 1.6
Portal vein	12.5 ± 3.2	19.3 ± 7.0 *	14.8 ± 5.0	11.6 ± 3.7	9.5 ± 2.8 *	8.1 ± 2.3 *
Renal vein	11.0 ± 3.0	17.2 ± 6.0 *	13.2 ± 4.4 *	10.5 ± 3.3	8.6 ± 1.9 *	6.4 ± 1.9 *
Renal Artery	11.8 ± 3.0	19.4 ± 6.7 *	14.8 ± 3.6 *	11.7 ± 3.6	9.6 ± 2.8 *	7.1 ± 2.2 *
Liver parenchyma	8.6 ± 2.2	10.5 ± 4.5	9.2 ± 3.5	8.3 ± 2.9	7.7 ± 2.3	5.8 ± 1.9 *
Pancreas parenchyma	6.8 ± 1.9	11.0 ± 3.9 *	8.8 ± 2.9 *	7.3 ± 2.3	6.3 ± 1.9	4.7 ± 1.4 *
Kidney (cortex)	13.2 ± 3.2	25.7 ± 10.1 *	19.2 ± 7.2 *	14.6 ± 5.2	11.6 ± 5.2 *	8.6 ± 2.9 *
CNR						
Primary tumor vs. urinary bladder wall	6.9 ± 1.8	11.2 ± 2.7 *	9.2 ± 2.2 *	7.7 ± 1.9	6.7 ± 1.6	6.6 ± 1.5
Primary tumor vs. renal cortex	4.9 ± 1.7	5.5 ± 2.3	4.2 ± 1.7	3.2 ± 1.2	2.5 ± 0.9 *	2.3 ± 0.9 *
Lymph node vs. retroperitoneal fat	13.2 ± 1.1	17.1 ± 1.4 *	14.8 ± 1.1 *	13.3 ± 0.9	12.4 ± 0.8	12.8 ± 0.8

comprises an excretory phase which allows for an accurate diagnostic assessment of the renal pelvis, ureter and bladder and a venous phase acquired to exclude distant metastases in patients with muscle-invasive disease [3]. This dual-scan approach does incur cumulative radiation dose, especially when applied repeatedly in follow-up CT examinations. One proposed way to bypass this problem is to use a single-scan, split bolus approach, in which two boluses of contrast media are administered aiming at the acquisition of a combined excretory/nephrographic scan [4,5]. However, this method implies a higher contrast media volume that needs to be injected which is suboptimal for patients with considerably impaired kidney function [6,7]. In a study by Metser et al., an intermediate phase 60 s after contrast media administration and supplemented by application of a diuretic was examined and a high diagnostic accuracy with regards to malignant urinary tract lesions was revealed [8]. However, assessment of organs and metastatic lesions was not investigated which could be hampered by iodine contrast deterioration occurring in late phase acquisitions and aggravating with increasing scan delay due to dispersion and renal elimination.

There are several technical approaches to Dual-energy CT (DECT) that have been shown to improve the diagnostic assessment of patients with urothelial carcinoma and other malignant diseases and to facilitate enhancement of iodine contrast by low keV monoenergetic reconstructions [9–13]. However, for a recent, detector-based spectral DECT [14], data on possible applications in genitourinary imaging are rather scarce.

We hypothesized that the decline of organ and vessel contrast encountered in excretory phase images could potentially be antagonized by the contrast enhancement provided by low keV reconstructions. Hence, the purpose of this pilot study was to investigate whether low keV virtual monoenergetic images of the excretory phase (excretory phase $VMI_{40\text{-}70\ keV}$) obtained with spectral DECT are feasible to maintain subjective assessability and quantitative image parameters of conventional venous phase CT and therefore hold the potential to be used in a single-scan, single-bolus approach.

2. Material and methods

This study was conducted with institutional review board approval. Informed patient consent was waived due to the retrospective character of the investigation. All scans were clinically indicated and not performed for the purpose of this study.

2.1. Patients

Identification of possible study patients was conducted based on a combined query to the picture archiving and communication system (PACS) and radiological information system (RIS) matching the criteria 1) age ≥18 years, 2) contrast-enhanced spectral DECT comprising late-venous and excretory phase between 06/01/2016 and 02/01/2018 and 3) histologically confirmed urothelial carcinoma (presurgical).

43 patients met these inclusion criteria. Of these patients, 16 were excluded due to lacking/inconclusive histopathologic report and a further patient due to an incomplete venous and excretory scan of the abdomen. Consequently, 26 patients were eligible for study inclusion.

2.2. Image acquisition

All scans were executed on a dual-energy spectral detector CT system (IQon, Philips Healthcare, Best, the Netherlands). After administration of a bodyweight-adapted volume of iodinated contrast media (< 55 kg: 1 ml/kg; 55–120 kg: 100 ml; > 120 kg: 120 ml; Accupaque 350 mg/ml, GE Healthcare (Chicago, IL)) via a peripheral vein,

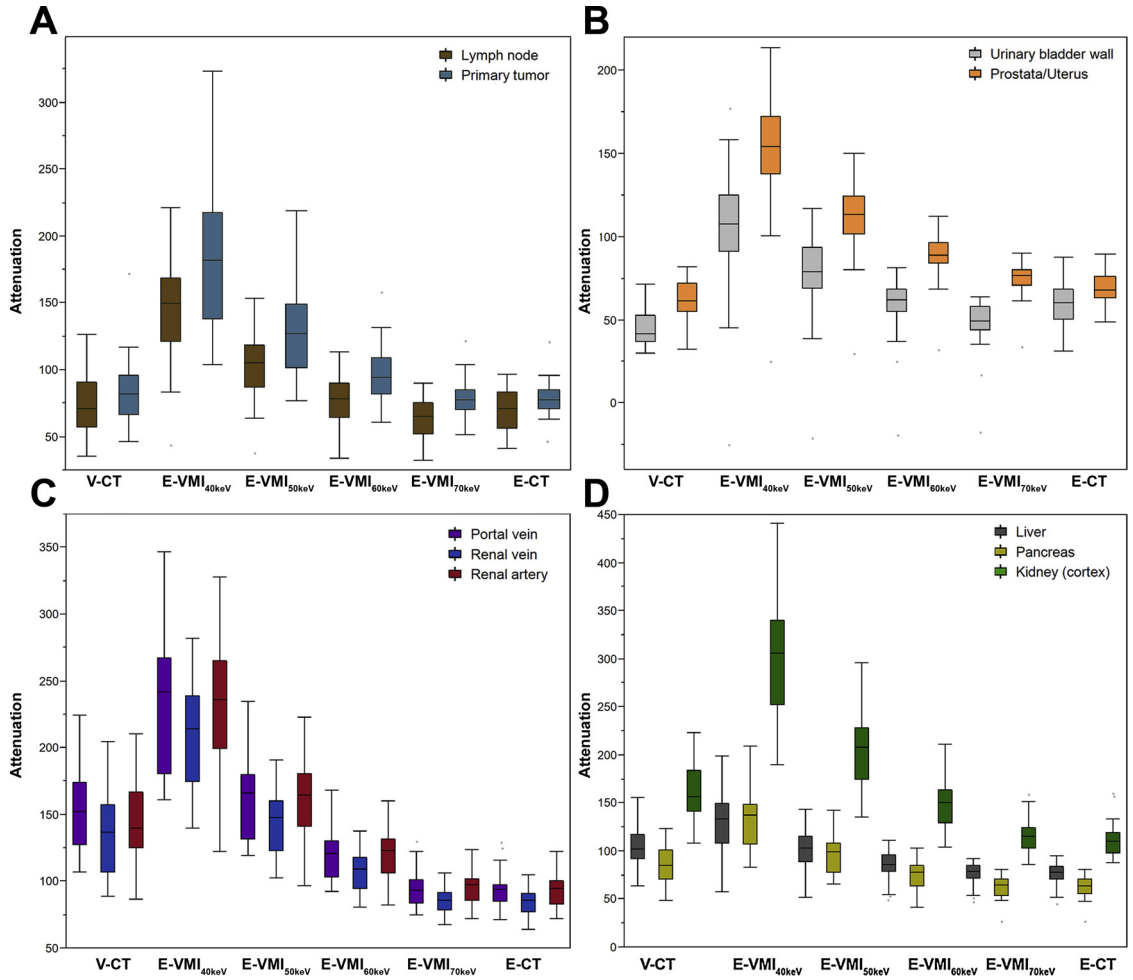

Fig. 1. Attenuation in lymph node, primary urothelial carcinoma, urinary bladder wall, prostate/uterus, portal/renal vein, renal artery, liver, pancreas and renal cortex in venous phase CT (V-CT), excretory phase $VMI_{40\text{-}70keV}$ (E-VMI) and excretory phase CT (E-CT).

followed by a 30 ml saline chaser (flow rate 3.5 ml/s), CT scans were carried out using the following parameters: tube current modulation activated (DoseRight 3D-DOM, Philips Healtcare, Best, The Netherlands), tube voltage 120 kVp, gantry rotation time 0.33 s, pitch 0.485, collimation 64 x 0.625 mm. Image acquisition started 50 and 240 s after the threshold of 150 HU in the descending aorta was attained for late-venous and excretory phase, respectively.

2.3. Post processing

All images were reconstructed in axial plane with a slice thickness of 2 mm and a section increment of 1 mm. For conventional venous- and excretory phase CT images, a hybrid-iterative reconstruction algorithm as used in clinical standard was applied (iDose 4, level 3, Rekon B, Philips Healthcare (Best, The Netherlands)). To obtain excretory phase VMI ranging from 40 to 70 keV with a stepwise increment of 10 keV, a dedicated, hybrid-iterative spectral algorithm with the same convolution kernel was used. Standard window settings for all reconstructions were a window level of 60 and a window width of 360.

2.4. Quantitative image analysis

For the included 26 patients, attenuation and standard deviation (SD) of the following regions were measured in venous and excretory phase CT and excretory phase VMI ranging from 40 to 70 keV by placing regions of interest (ROI) in the following areas: primary tumor, liver parenchyma (right liver lobe, excluding large vessels), pancreatic corpus, renal cortex, anterior wall of urinary bladder, lymph node (at the section of maximum diameter), prostate or uterus, portal vein, renal artery, renal vein, psoas muscle and subcutaneous fat (both at the level of the first lumbar vertebra). ROIs for primary tumor and metastases were drawn at the slice of the largest lesion diameter in order to cover a maximum area. All organ parenchyma and vessel ROIs were drawn in order to reflect the largest parenchyma/vessel lumen possible without including non-relevant tissue.

2.5. Qualitative assessment

Three independent radiologists with 2, 3 and 8 years of experience subjectively assessed venous phase CT, excretory phase CT and excretory phase VMI ranging from 40 to 70 keV regarding the following criteria using 5-point Likert scales:

1) Vessel contrast in renal artery, renal vein and portal vein (1 = low vessel contrast, poor interpretability of vessel lumen; 5 = excellent vessel contrast, clearly assessable vessel lumen),
2) Delineation of the primary tumor (1 = lacking delineation with poor contrast to circumjacent tissue 5 = ideal lesion delineation with strong lesion contrast),
3) Delineation of distant metastases (1 = lacking delineation with poor contrast to circumjacent tissue 5 = ideal lesion delineation with strong lesion contrast).
4) Diagnostic certainty regarding metastatic origin of those lesions (1 = uncertain, unclear lesion dignity; 5 = highly confident,

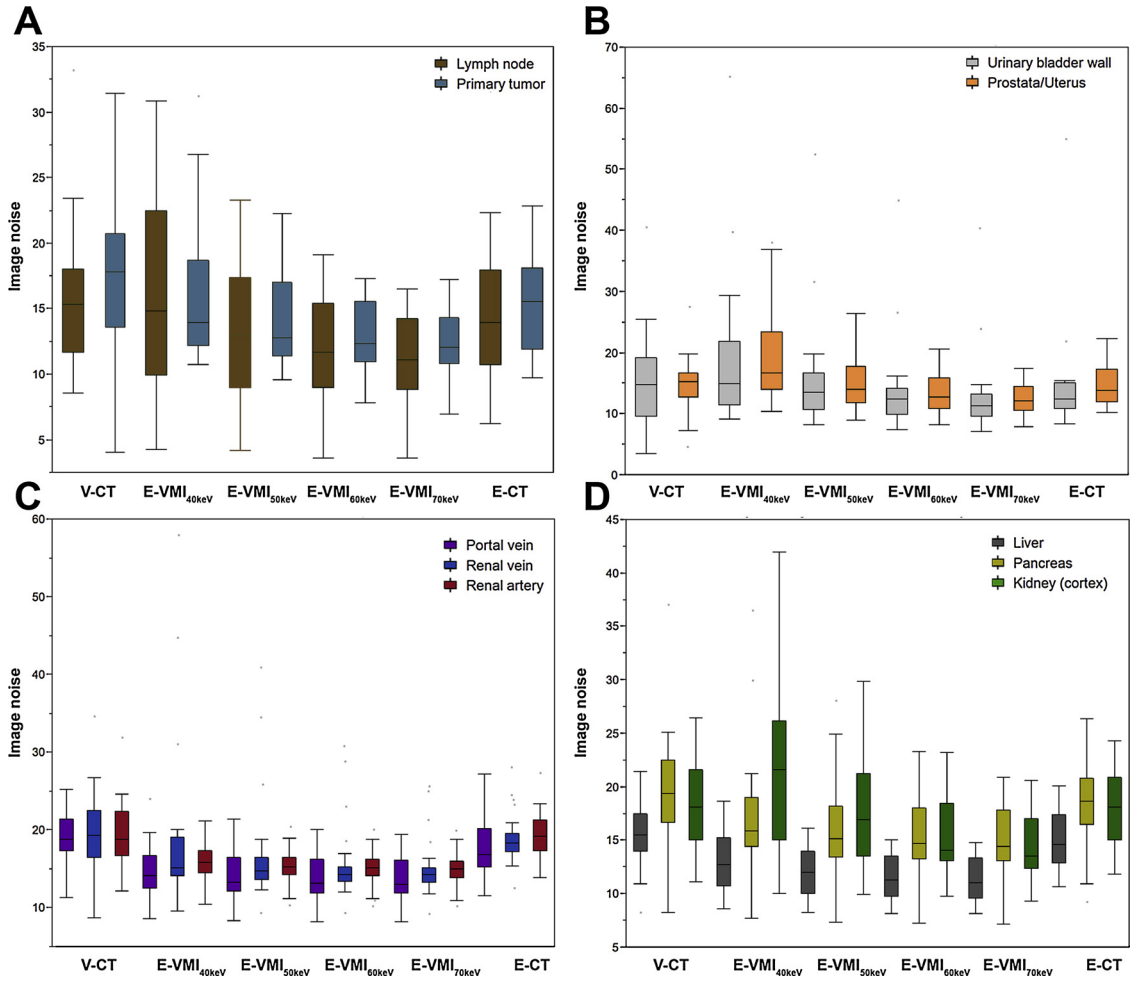

Fig. 2. Image noise in lymph nodes, primary urothelial carcinoma, urinary bladder wall, prostate/uterus, portal/renal vein, renal artery, liver, pancreas and renal cortex in venous phase CT (V-CT), excretory phase $VMI_{40\text{-}70keV}$ (E-VMI) and excretory phase CT (E-CT).

definitely a metastasis).

Metastatic lesions were annotated beforehand and correlated to a standard of reference (prior or follow-up CT and/or MRI). The subjective readers were provided with the slice position and exact localization of primary tumors and metastases.

2.6. Statistical methods

SNR of a $ROI_{(x)}$ and CNR to the surrounding $tissue_{(y)}$ were calculated as reported earlier [15]:

$$SNRx = \frac{HUx}{SDx}$$

$$CNR = \frac{|HUx - HUy|}{\sqrt[2]{SDx + SDy}}$$

Non-parametric Wilcoxon Test with Steel-Dwass method to adjust for multiple comparison was conducted to analyze subjective Likert scores and quantitative values using JMP software (Version 13, SAS Institute, Cary, USA).

Interrater variability was analyzed with the intraclass correlation coefficient (ICC) which was interpreted as follows: excellent agreement ($\kappa \geq 0.8$), good agreement ($\kappa \geq 0.6$), moderate agreement ($\kappa \geq 0.4$), poor agreement ($\kappa \leq 0.4$). Statistical significance was defined as $p \leq 0.05$. Continuous variables are reported as mean ± standard deviation (SD) while Likert scores are listed as median and inter-quartile range.

3. Results

3.1. Study cohort

Of the 26 included patients, 6 were female (mean age: 52.5 ± 5.4 years) and 20 were male (mean age: 46.4 ± 9.5 years). In 14 patients, urothelial carcinoma was localized within the urinary bladder, in 11 patients within the renal pelvis and in one patient within the urethra. 10 out of 26 patients suffered from metastatic disease from which 19 lymph node, 16 liver, 2 soft tissue and one peritoneal metastases were included. Mean CTDI was 12.2 ± 4.6 mGy for the portal venous scan and 11.9 ± 4.1 mGy for the excretory DECT.

3.2. Quantitative image analysis

Attenuation in excretory phase VMI_{40keV} was significantly higher compared to venous phase CT in all tested ROIs ($p < 0.001$) except for liver parenchyma where it was comparable ($p = 0.07$). In urinary bladder wall, attenuation was higher in excretory phase CT ($p \leq 0.05$) compared to venous phase CT while for lymph nodes, primary tumor and prostate/uterus, it was comparable (p-range: 0.34 − 0.99). For all other ROIs, attenuation in excretory phase CT was significantly lower than in venous phase CT ($p < 0.001$). Pertaining to image noise, there was no significant difference between venous phase CT and excretory phase VMI_{40keV} (p-range: 0.08–1.00), except for liver, portal vein and renal artery, where it was significantly lower in $VMI40_{keV}$ ($p \leq 0.05$; Fig. 2). SNR was comparable in excretory phase VMI_{40keV} and venous

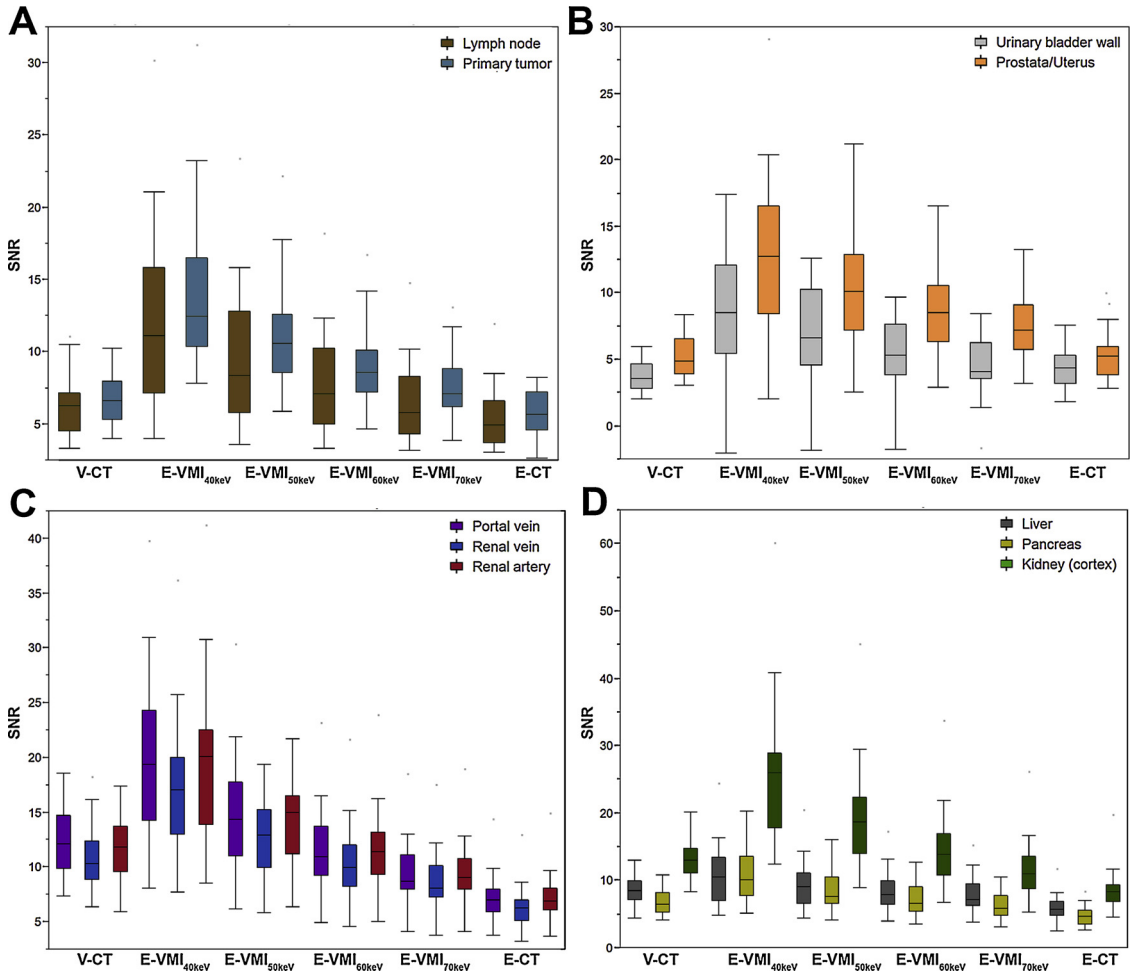

Fig. 3. SNR in lymph nodes, primary tumor, urinary bladder wall, prostate/Uterus, portal/renal vein, renal artery, liver, pancreas and renal cortex in venous phase CT (V-CT), excretory phase $VMI_{40\text{-}70keV}$ (E-VMI) and excretory phase CT (E-CT).

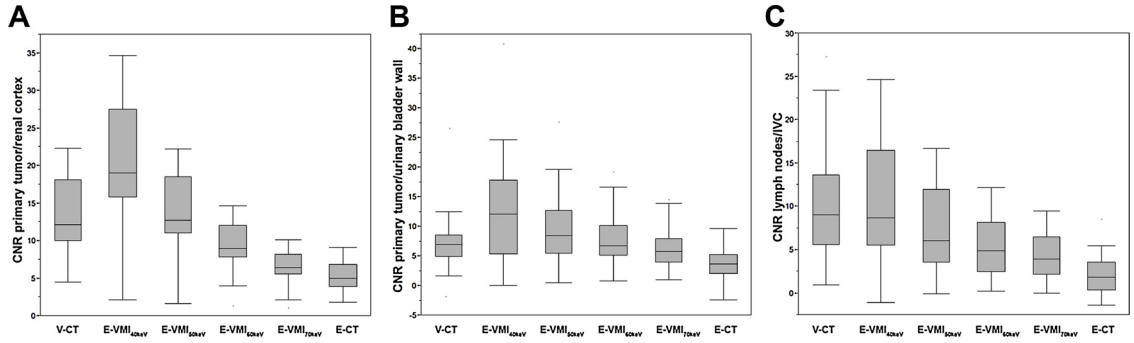

Fig. 4. Contrast-to-noise ratio (CNR) of primary urothelial carcinoma vs. renal cortex and urinary bladder wall as well as lymph nodes vs. inferior vena cava.

Table 2
Mean Likert scores for delineation of primary tumor and metastasis, diagnostic certainty regarding metastatic lesion dignity as well as subjective vessel contrast of portal and renal vein as well as renal artery. Asterisks indicate statistical significance compared to venous phase CT.

	Venous-phase CT	Excretory-phase VMI_{40keV}	Excretory-phase VMI_{50keV}	Excretory-phase VMI_{60keV}	Excretory-phase VMI_{70keV}	Excretory-phase CT
Delineation						
Primary tumor Metastasis	4 (3-4.5) 4 (3-5)	4 (3-5) * 4 (4-5) *	4 (3-5) 4 (3-4)	3.5 (2-4) 3 (3-4) *	3 (2-4) * 3 (2-4) *	3 (3-4) 3 (2-4) *
Diagnostic certainty*Metastasis*	4 (3-5)	4 (3-5)	4 (3-4)	3 (2.75-4) *	3 (2-4) *	3 (2-4) *
Vessel contrast						
Portal vein	4 (3-5)	4 (4-5) *	4 (3-4)	3 (2-3) *	2 (2-3) *	2 (1-3) *
Renal vein	4 (4-5)	5 (4-5) *	4 (3-4)	3 (3-4) *	2 (2-3) *	2 (1-3) *
Renal artery	4 (3-5)	4 (4-5) *	4 (3-4)	3 (2-3) *	2 (1-3) *	2 (1-3) *

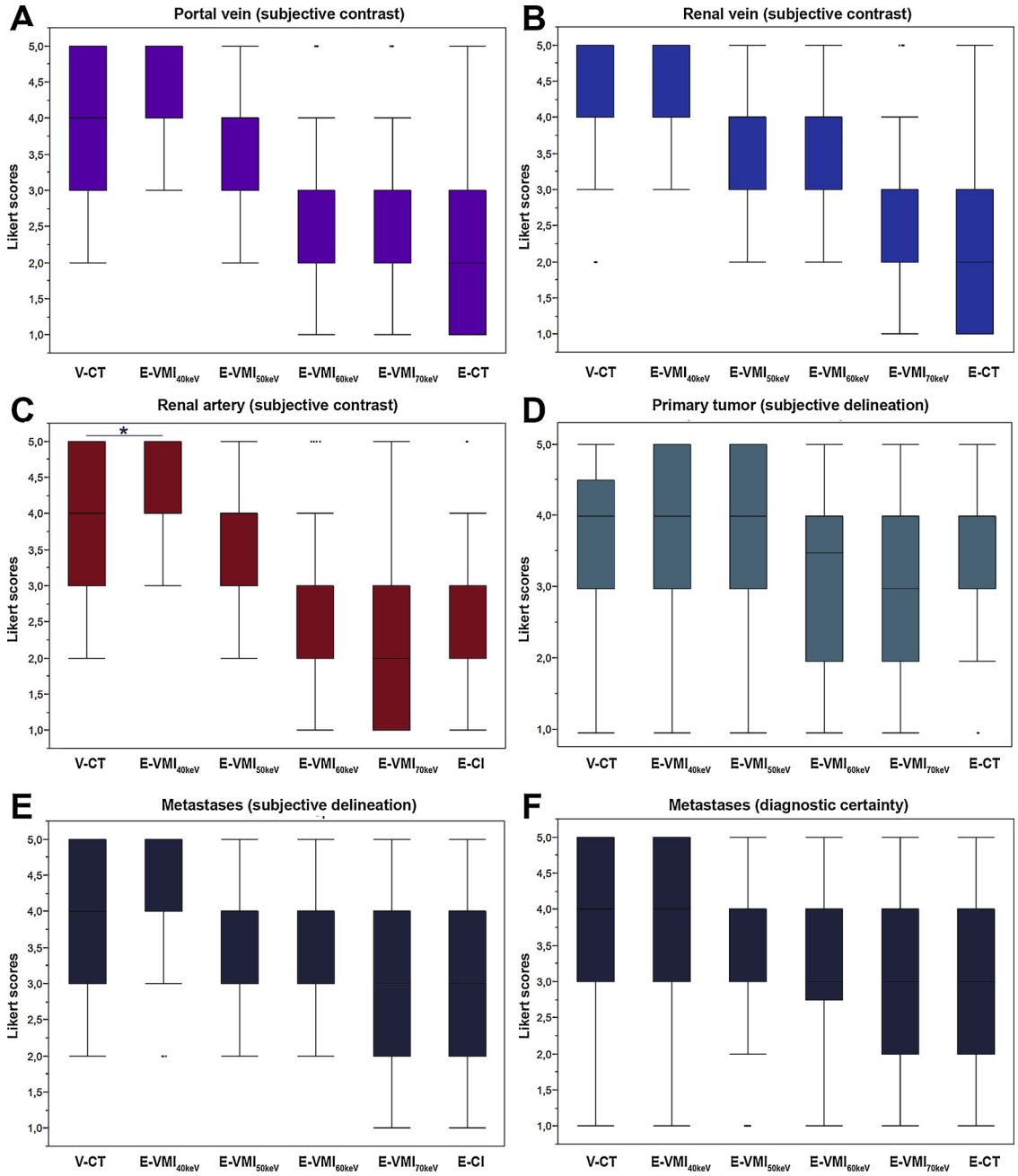

Fig. 5. Likert scores for subjective contrast of portal (A) and renal vein (B), renal artery (C) delineation of primary urothelial carcinoma (D) and metastases (E) as well as diagnostic certainty (F) in venous phase CT (V-CT), excretory phase $VMI_{40\text{-}70keV}$ (E-VMI) and excretory phase CT (E-CT).

phase CT regarding liver parenchyma ($p = 0.17$) while in all other tested ROIs, it was highest in excretory phase VMI_{40keV} ($p < 0.01$). Urinary bladder wall, lymph node, primary tumor and prostate/uterus showed a comparable SNR in excretory phase CT and venous phase CT (p-range: 0.11 − 0.82) while for liver parenchyma, portal and renal vein, renal artery, pancreas and renal cortex, SNR was significantly lower in excretory phase CT compared to venous phase CT ($p < 0.001$). Regarding CNR, excretory phase VMI_{40keV} were superior to venous phase CT ($p < 0.001$) for contrast between lymph nodes and retroperitoneal fat (excretory phase VMI_{40keV}/VCI: 17.1 ± 1.4 vs. 13.2 ± 1.1) as well as primary tumor vs. urinary bladder wall (excretory phase VMI_{40keV}/VCI: 11.2 ± 2.7 vs. 6.9 ± 1.8). CNR of primary tumor vs. renal cortex was similar in excretory phase VMI_{40keV} compared to venous phase CT (excretory phase VMI_{40keV}/VCI: 5.5 ± 2.3 vs. 4.9 ± 1.7; $p = 1.00$). Quantitative values for attenuation, SNR and CNR are pointed out in detail in Table 1 and illustrated in Figs. 1, 3 and 4, respectively.

3.3. Qualitative assessment

Qualitative image assessment revealed that delineation (VMI_{40keV}: 4(4–5) vs. venous phase CT: 4(3–5)) and diagnostic certainty (VMI_{40keV}: 4(3–5) vs. venous phase CT: 4(3–5)) regarding metastatic lesions as well as delineation of primary tumor (VMI_{40keV}: 4(3–5) vs. venous phase CT: 4(3–4.5)) and subjective vessel contrast of renal artery (VMI_{40keV}: 4(4–5) vs. venous phase CT: 4(3–5)) and portal vein (VMI_{40keV}: 4(4–5) vs. venous phase CT: 4(3–5)) received comparable Likert scores in venous phase CT and excretory phase VMI_{40keV} (p-range: 0.42–1.00). Solely, subjective contrast of renal vein (VMI_{40keV}: 4(4–5) vs. C-VI: 4(4–5)) received slightly better average ratings in

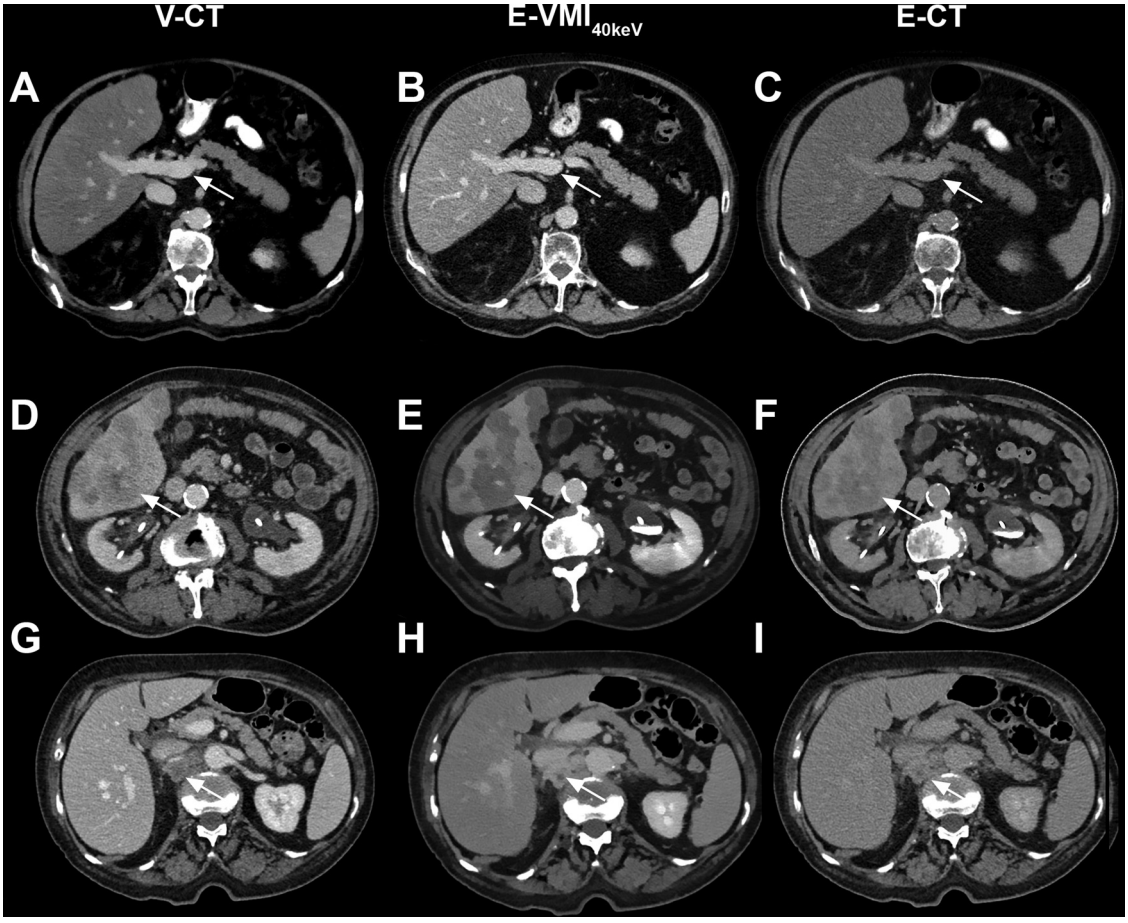

Fig. 6. Image examples illustrating the iodine contrast boost at excretory phase VMI_{40keV} antagonizing the organ/vessel contrast deterioration in excretory phase images, resulting in a comparable contrast compared to C-VI: portal vein (A–C), liver metastases (D–F), lymph node metastases (G–I). Standard window width and level were used (L = 60/ W = 360).

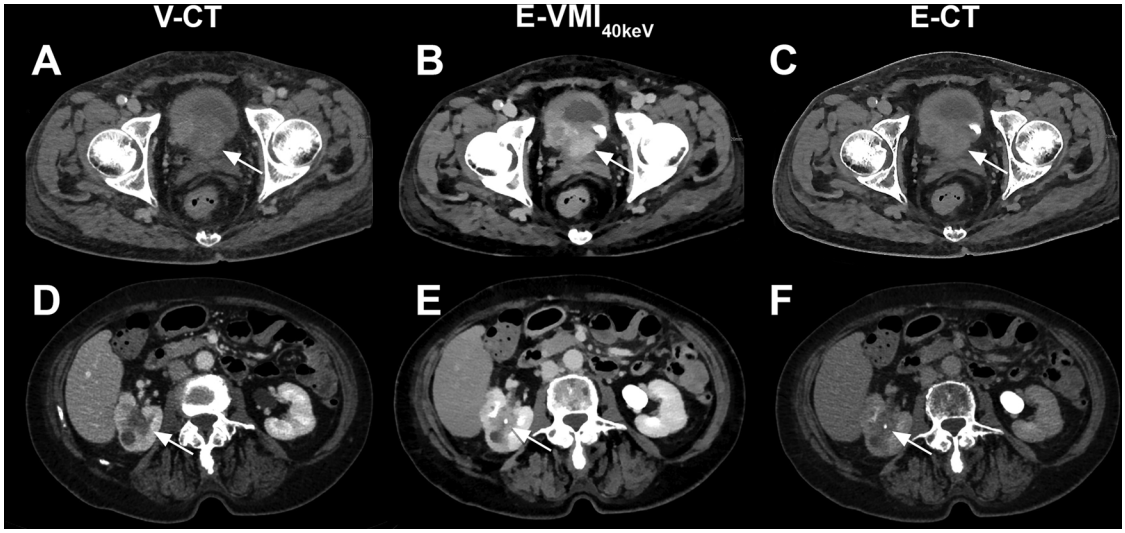

Fig. 7. Axial plane sections showing primary tumor manifestations of urothelial carcinoma allocated in the posterior urinary bladder wall (A–C) and the right renal pelvis (G–I). Excretory-phase VMI_{40keV} show the clearly enhanced contrast compared to C-VI. Standard window width and level were used (L = 60/ W = 360).

excretory phase VMI_{40keV} compared to venous phase CT ($p = 0.04$). Mean Likert scores for excretory phase VMI at 50–70 keV decreased with rising keV levels in all 5 categories and were significantly lower in excretory phase VMI_{70keV} compared to venous phase CT except for primary tumor delineation ($p \leq 0.05$ and $p = 0.12$, respectively). Compared to venous phase CT, excretory phase CT was rated lower with regards to metastasis delineation and diagnostic certainty as well as subjective contrast for all assessed vessels ($p < 0.001$) while primary tumor delineation was rated equal ($p = 0.62$). Between all three readers, interobserver agreement regarding the qualitative assessment was moderate (ICC = 0.44) for venous phase CT and excretory phase $VMI_{40\text{-}70keV}$, while for conventional excretory phase images, it was poor

(ICC = 0.37). The detailed results of the qualitative assessment given in Table 2. Figs. 6 and 7 show exemplary axial plane images comparing excretory phase $VMI4_{0keV}$, venous and excretory phase CT of primary tumors, vessels and different metastatic manifestations.

4. Discussion

In this feasibility study, we compared quantitative and qualitative criteria of low keV virtual monoenergetic images obtained from excretory-phase spectral dual energy computed tomography with conventional venous phase images. Compared to venous phase CT, the quantitative image analysis of parenchymal organs, arterial and venous vessels, renal cortex, bladder wall as well as primary urothelial tumor manifestations demonstrated comparable or even higher values for attenuation (Fig. 1), SNR (Fig. 3) and CNR (Fig. 4) in excretory phase VMI_{40keV}. In the qualitative analysis, renal vein contrast received superior Likert scores in excretory phase VMI_{40keV} compared to venous phase CT while delineation of primary urothelial carcinomas and metastases, diagnostic certainty regarding metastatic lesion dignity as well as subjective vessel contrast of renal artery and portal vein were rated equally (Fig. 5, Table 2).

These results illustrate that the iodine contrast boost achieved by VMI_{40keV} effectively antagonizes the deterioration of organ/vessel contrast naturally occurring in the excretory phase resulting in a comparable subjective assessability as provided by conventional venous phase images. However, the overall interobserver agreement was only moderate for venous phase CT and excretory phase VMI_{40keV} and poor for excretory phase CT which could be explained by the fact that the readers were not used to employ excretory phase images for assessing parenchymal organs, vessels or distant metastases, possibly leading to a certain level of interobserver variability.

Contrast-enhanced venous phase CT of the abdomen and pelvis plays an important role for the pretreatment staging of patients with urothelial carcinoma as it facilitates detection of extravesical/extraluminal tumor growth as well as lymphatic and hematogenous metastases [16–18]. Staging protocols usually comprise an additional excretory phase scan acquired 4–6 min after contrast media injection in order to rule out multifocal lesions of the upper urinary tract for which it attains a sensitivity of 50–70% [19]. As multiphasic scans cumulate in a high overall radiation dose, different modified protocols have been investigated in the past in order to reduce applied radiation dose while maintaining a comparable diagnostic accuracy in the assessment of malignant lesions of the upper and lower urinary tract on the one hand and local/distant metastases on the other: In the split bolus approach, a second bolus of contrast media is applied 5 min after the initial injection resulting in the acquisition of a combined excretory/nephrographic or excretory/venous phase phase, depending on the chosen delay [4,20,5]. Reported sensitivity for upper urinary tract tumors ranges from 80 to 100%, yet the necessity of additional contrast media injection implies additional health care expenses and may be unsuitable for patients with reduced kidney function [21–23,20,4]. By contrast, Metser et al. focused on a different approach using a single intermediate-urothelial phase protocol in which image acquisition took place 60 s after administration of contrast agent and previous application of a diuretic [8]. The intermediate phase was reported to yield an optimal opacification of the urinary tract and was therefore valued as a promising approach with a diagnostic accuracy for malignant urinary tract lesions comparable to established scan protocols (sensitivity of 82.6% for primary urothelial carcinomas). However, the assessment of lymph node or hematogenous (*e.g.* liver) metastases was not evaluated, which might be hampered by lesion, organ and vessel contrast deterioration in the proposed intermediate phase. Hence, the focus of our proof-of-concept study was to evaluate if low keV imaging could be utilized to prevent the decline of iodine contrast in excretory phase images and therefore bypass a possible trade-off between ureter opacification and optimal lesion/organ assessment. Our results suggest these low keV reconstructions as suitable for a combined approach with intermediate phase images as suggested by Metser et al. which would imply significant dose savings without the necessity of a second contrast media administration as performed in the split bolus approach. In contrast to our work, previous studies investigating the diagnostic value of dual-energy CT in the field of urothelial carcinoma were primarily focused on comparing virtual with true unenhanced images or tumor compartmentalization based on material separation [24–26]. However, the improved subjective and objective image parameters we discovered for excretory phase VMI_{40keV} compared to conventional excretory phase CT are concordant with the results revealed by previous studies that investigated lesion depiction [13,27,28] or CT angiography [29,30] in the abdomen.

Besides its retrospective character and the rather small sample size investigated, there are limitations to this pilot study that need to be addressed. Evaluating opacification or qualitative assessment of the ureter was not investigated for two reasons: First, it is known that diagnostic accuracy for ureteral tumor lesions is already excellent in conventional images [8]; iodine contrast boost in low keV virtual monoenergetic images would probably lead to strong blooming artifacts superimposing the ureter so that conventional images would remain necessary for its accurate diagnostic assessment. Second, in our patient cohort, there were no patients with ureteral tumor lesions that could have allowed for detailed analysis of diagnostic accuracy to this regard. As another limitation, the patient cohort included in our study is rather small hence subgroup analysis of different metastatic lesions regarding the qualitative assessment was not possible. Moreover, it is known that low energy VMI can affect size measurements especially in small tumor volumes [31] which might be relevant for smaller ureteral lesions, yet was not investigated here. Last, in this proof-of concept study, we showed a comparable or even improved subjective delineation of metastatic lesions but refrained from analyzing their detection rate and quantitative image parameters due to the small sample size and heterogenous metastatic sites. This aspect should be assessed in a subsequent trial as characteristic enhancement patterns may obscure liver metastases at longer scan delays. However, this potential issue partially accounts for the split-bonus technique as well.

5. Conclusions

In conclusion, the results of this pilot study indicate that low-energy virtual monoenergetic reconstructions could be a feasible method to maintain vessel, organ and tumor contrast in excretory phase images in patients with urothelial carcinoma resulting in a subjective assessability comparable to venous phase images. When further evaluating these reconstructions, *e.g.* in a single-scan, single-bolus approach as suggested by Metser et al., the diagnostic accuracy regarding distant metastases should be investigated systematically.

Funding

This work was funded through the Else Kröner-Fresenius Stiftung (2016-Kolleg-19 to Simon Lennartz). The funding source hat no involvement in study design, the collection, analysis and interpretation of data or in the writing of the report.

Conflict of interest

The authors of this manuscript declare relationships with the following companies: David Maintz, Jan Borggrefe and Nils Große Hokamp: received speakers' honoraria from Philips Healthcare. Simon Lennartz: received exemption from clinical duties for research outside this specific project as a part of a research agreement between Philips Healthcare and University Hospital Cologne; received travel cost reimbursement from Philips Healthcare. Daniel Pinto Dos Santos received consulting fees not related to this project from Cook Medical.

References

[1] M. Ploeg, K.K.H. Aben, L.A. Kiemeney, The present and future burden of urinary bladder cancer in the world, World J. urol. 27 (2009) 289–293, https://doi.org/10.1007/s00345-009-0383-3.

[2] L.-J. Wang, Y.-C. Wong, C.-C. Huang, C.-H. Wu, S.-C. Hung, H.-W. Chen, Multidetector computerized tomography urography is more accurate than excretory urography for diagnosing transitional cell carcinoma of the upper urinary tract in adults with hematuria, J. Urol. 183 (2010) 48–55, https://doi.org/10.1016/j.juro.2009.08.144.

[3] S.S. Chang, B.H. Bochner, R. Chou, R. Dreicer, A.M. Kamat, S.P. Lerner, et al., Treatment of Non-metastatic muscle-invasive bladder cancer: AUA/ASCO/ASTRO/SUO guideline, J. Urol. 198 (2017) 552–559, https://doi.org/10.1016/j.juro.2017.04.086.

[4] H. Shaish, J.H. Newhouse, Split-bolus CT urogram: Is less more? Abdominal Radiol. 42 (2017) 2119–2126, https://doi.org/10.1007/s00261-017-1098-3.

[5] C.-Y. Chen, J.-S. Hsu, T.-S. Jaw, Shih M-CP, L.-J. Lee, T.-H. Tsai, G.-C. Liu, Split-bolus Portal venous phase dual-energy CT urography: protocol design, image quality, and dose reduction. AJR, Am. J. Roentgenol. 205 (2015) W492–501, https://doi.org/10.2214/AJR.14.13687.

[6] M.S. Davenport, R.H. Cohan, J.H. Ellis, Contrast media controversies in 2015: imaging patients with renal impairment or risk of contrast reaction, AJR. Am. J. Roentgenol. 204 (2015) 1174–1181, https://doi.org/10.2214/AJR.14.14259.

[7] L. Gruberg, G.S. Mintz, R. Mehran, G. Dangas, A.J. Lansky, K.M. Kent, et al., The prognostic implications of further renal function deterioration within 48 h of interventional coronary procedures in patients with pre-existent chronic renal insufficiency, J. Am. Coll. Cardiol. 36 (2000) 1542–1548, https://doi.org/10.1016/S0735-1097(00)00917-7.

[8] U. Metser, M.A. Goldstein, T.P. Chawla, N.E. Fleshner, L.M. Jacks, M.E. O'Malley, Detection of urothelial tumors: comparison of urothelial phase with excretory phase CT urography–a prospective study, Radiology 264 (2012) 110–118, https://doi.org/10.1148/radiol.12111623.

[9] C. Hansen, C.D. Becker, X. Montet, D. Botsikas, Diagnosis of urothelial tumors with a dedicated dual-source dual-energy MDCT protocol: preliminary results, AJR. Am. J. Roentgenol. 202 (2014) W357–64, https://doi.org/10.2214/AJR.13.11145.

[10] Cecco C.N. de, D. Caruso, U.J. Schoepf, Santis D. de, G. Muscogiuri, M.H. Albrecht, et al., A noise-optimized virtual monoenergetic reconstruction algorithm improves the diagnostic accuracy of late hepatic arterial phase dual-energy CT for the detection of hypervascular liver lesions, Eur. Radiol. 28 (2018) 3393–3404, https://doi.org/10.1007/s00330-018-5313-6.

[11] S. Lennartz, M. Le Blanc, D. Zopfs, N. Große Hokamp, N. Abdullayev, K.R. Laukamp, et al., Dual-energy CT-derived iodine maps: use in assessing pleural carcinomatosis, Radiology (2019) 181567, , https://doi.org/10.1148/radiol.2018181567.

[12] D. Zopfs, S. Lennartz, K. Laukamp, N. Große Hokamp, A. Mpotsaris, D. Maintz, et al., Improved depiction of atherosclerotic carotid artery stenosis in virtual monoenergetic reconstructions of venous phase dual-layer computed tomography in comparison to polyenergetic reconstructions, Eur. J. Radiol. 100 (2018) 36–42, https://doi.org/10.1016/j.ejrad.2018.01.008.

[13] N. Große Hokamp, A.J. Höink, J. Doerner, D.W. Jordan, G. Pahn, T. Persigehl, et al., Assessment of arterially hyper-enhancing liver lesions using virtual monoenergetic images from spectral detector CT: phantom and patient experience, Abdominal Radiol. 43 (2018) 2066–2074, https://doi.org/10.1007/s00261-017-1411-1 New York.

[14] C.H. McCollough, S. Leng, L. Yu, J.G. Fletcher, Dual- and multi-energy CT: principles, technical approaches, and clinical applications, Radiology 276 (2015) 637–653, https://doi.org/10.1148/radiol.2015142631.

[15] V. Neuhaus, N. Abdullayev, N. Große Hokamp, G. Pahn, C. Kabbasch, A. Mpotsaris, et al., Improvement of image quality in unenhanced dual-layer CT of the head using virtual monoenergetic images compared with polyenergetic single-energy CT, Invest. Radiol. 52 (2017) 470–476, https://doi.org/10.1097/RLI.0000000000000367.

[16] J. Zhang, S. Gerst, R.A. Lefkowitz, A. Bach, Imaging of bladder cancer, Radiologic clinics of North America 45 (2007) 183–205, https://doi.org/10.1016/j.rcl.2006.10.005.

[17] A.D. Macvicar, Bladder cancer staging, BJU Int. 86 (2000) 111–122, https://doi.org/10.1046/j.1464-410X.2000.00589.x.

[18] S.B. Park, J.K. Kim, H.J. Lee, H.J. Choi, K.-S. Cho, Hematuria: Portal venous phase multi detector row CT of the bladder–a prospective study, Radiology 245 (2007) 798–805, https://doi.org/10.1148/radiol.2452061060.

[19] M. Jinzaki, K. Matsumoto, E. Kikuchi, K. Sato, Y. Horiguchi, Y. Nishiwaki, S.G. Silverman, Comparison of CT urography and excretory urography in the detection and localization of urothelial carcinoma of the upper urinary tract, AJR. Am. J. Roentgenol. 196 (2011) 1102–1109, https://doi.org/10.2214/AJR.10.5249.

[20] E. Maheshwari, M.E. O'Malley, S. Ghai, M. Staunton, C. Massey, Split-bolus MDCT urography: Upper tract opacification and performance for upper tract tumors in patients with hematuria, AJR. Am. J. Roentgenol. 194 (2010) 453–458, https://doi.org/10.2214/AJR.09.3228.

[21] M. Tepel, P. Aspelin, N. Lameire, Contrast-induced nephropathy: a clinical and evidence-based approach, Circulation 113 (2006) 1799–1806, https://doi.org/10.1161/CIRCULATIONAHA.105.595090.

[22] R. Solomon, W. Dumouchel, Contrast media and nephropathy: findings from systematic analysis and food and drug administration reports of adverse effects, Invest. Radiol. 41 (2006) 651–660, https://doi.org/10.1097/01.rli.0000229742.54589.7b.

[23] J.L. Gross, R. Friedman, S.P. Silveiro, Preventing nephropathy induced by contrast medium, New Engl. J. Med. 354 (2006) 1853–1855, https://doi.org/10.1056/NEJMc060405 author reply 1853-5.

[24] G. Ascenti, A. Mileto, M. Gaeta, A. Blandino, S. Mazziotti, E. Scribano, Single-phase dual-energy CT urography in the evaluation of haematuria, Clin. Radiol. 68 (2013) e87–94, https://doi.org/10.1016/j.crad.2012.11.001.

[25] P. Durieux, P.A. Gevenois, A. van Muylem, N. Howarth, C. Keyzer, Abdominal attenuation values on virtual and true unenhanced images obtained with Third-generation dual-source dual-energy CT, AJR. Am. J. Roentgenol. 210 (2018) 1042–1058, https://doi.org/10.2214/AJR.17.18248.

[26] H. Mirka, J. Baxa, M. Hora, O. Hes, O. Topolcan, J. Ferda, Iodine content analysis using dual-energy computed tomography as a biomarker of transitional cell carcinoma, an experience with separation of the clotted blood and tumorous tissue, Anticancer Res. 38 (2018) 541–545, https://doi.org/10.21873/anticanres.12256.

[27] Cecco C.N. de, D. Caruso, U.J. Schoepf, J.L. Wichmann, J.R. Ter Louw, J.D. Perry, et al., Optimization of window settings for virtual monoenergetic imaging in dual-energy CT of the liver: a multi-reader evaluation of standard monoenergetic and advanced imaged-based monoenergetic datasets, Eur. J. Radiol. 85 (2016) 695–699, https://doi.org/10.1016/j.ejrad.2016.01.007.

[28] S.S. Martin, S. Pfeifer, J.L. Wichmann, M.H. Albrecht, D. Leithner, L. Lenga, et al., Noise-optimized virtual monoenergetic dual-energy computed tomography: optimization of kiloelectron volt settings in patients with gastrointestinal stromal tumors, Abdominal radiology (New York) 42 (2017) 718–726, https://doi.org/10.1007/s00261-016-1011-5.

[29] M.H. Albrecht, J. Trommer, J.L. Wichmann, J.-E. Scholtz, S.S. Martin, T. Lehnert, et al., Comprehensive comparison of virtual monoenergetic and linearly blended reconstruction techniques in Third-generation dual-source dual-energy computed tomography angiography of the thorax and abdomen, Invest. Radiol. 51 (2016) 582–590, https://doi.org/10.1097/RLI.0000000000000272.

[30] M.H. Albrecht, J.-E. Scholtz, K. Hüsers, M. Beeres, A.M. Bucher, M. Kaup, et al., Advanced image-based virtual monoenergetic dual-energy CT angiography of the abdomen: optimization of kiloelectron volt settings to improve image contrast, Eur. Radiol. 26 (2016) 1863–1870, https://doi.org/10.1007/s00330-015-3970-2.

[31] A.M. den Harder, F. Bangert, R.W. van Hamersvelt, T. Leiner, J. Milles, A.M.R. Schilham, et al., The effects of iodine attenuation on pulmonary nodule volumetry using novel dual-layer computed tomography reconstructions, Eur. Radiol. 27 (2017) 5244–5251, https://doi.org/10.1007/s00330-017-4938-1.